SCIENCE CHINA
Physics, Mechanics & Astronomy

• Article •

October 2012 Vol. 55 No. 10: 1832–1843
doi: 10.1007/s11433-012-4880-9

A novel smooth and discontinuous oscillator with strong irrational nonlinearities

HAN YanWei[1], CAO QingJie[1,2*], CHEN YuShu[1] & WIERCIGROCH Marian[3]

[1]*School of Astronautics, Harbin Institute and Technology, Harbin 150001, China;*
[2]*Department of Mathematics and Physics, Shijiazhuang Tiedao University, Shijiazhuang 050043, China;*
[3]*Centre for Applied Dynamics Research, School of Engineering, University of Aberdeen, King's College, Aberdeen AB24 3UE, Scotland, UK*

Received July 7, 2011; accepted February 23, 2012; published online August 27, 2012

In this paper, we propose a novel nonlinear oscillator with strong irrational nonlinearities having smooth and discontinuous characteristics depending on the values of a smoothness parameter. The oscillator is similar to the SD oscillator, originally introduced in Phys Rev E 69(2006). The equilibrium stability and the complex bifurcations of the unperturbed system are investigated. The bifurcation sets of the equilibria in parameter space are constructed to demonstrate transitions in the multiple well dynamics for both smooth and discontinuous regimes. The Melnikov method is employed to obtain the analytical criteria of chaotic thresholds for the singular closed orbits of homoclinic, homo-heteroclinic, cuspidal heteroclinic and tangent homoclinic orbits of the perturbed system.

irrational nonlinearity, multiple well dynamics, singular closed orbits, Melnikov method

PACS number(s): 05.45.-a, 05.45.Gg, 05.45.Pq

Citation: Han Y W, Cao Q J, Chen Y S, et al. A novel smooth and discontinuous oscillator with strong irrational nonlinearities. Sci China-Phys Mech Astron, 2012, 55: 1832–1843, doi: 10.1007/s11433-012-4880-9

1 Introduction

Classical mechanical oscillators play an important role in modern science and technology and they have been extensively applied in engineering [1–5], molecular biology [6,7], lattice dynamics [8,9] and quantum mechanics [10]. In the past few decades, much attention has been paid to nonlinear systems which are used to model and analyze the practical systems. For example, Dupac et al. [11] modeled an electromagnetically levitated droplet as a three-dimensional system with lumped masses and elastic springs where its nonlinear behaviour was investigated. Kaper et al. [12] studied the behaviour of an oscillator having a discontinuous dynamic vibration absorber. Boubaker et al. [13] investigated the mesoscopic fabric models by employing a discrete mass-spring approach. Terumichi et al. [14] proposed a mass-spring system attached at the lower end to a time-varying length string and the nonstationary vibrations were investigated.

Recently, Cao et al. [15–21] have proposed and investigated a smooth and discontinuous (SD) oscillator to study transitions from smooth to discontinuous dynamics being controlled by a parameter α. The oscillator is an example of a conservative nonlinear oscillatory system in which the restoring force can have an irrational form. The generalized complete elliptic integrals of the first and the second kind have been introduced in ref. [20] to investigate the Hopf bifurcations of the system, where the details of this work can be found. A highly accurate solution for the SD oscillator was obtained by a generalized Senator-Bapat perturbation technique in ref. [22]. It is worth pointing out that the restoring force in the SD oscillator is a single irrational nonlinearity having one switch point for the snap-through buckling at which a transition occurs from single well to double well dynamics, as can be seen in ref. [15]. This switch point itself is degenerate singular having codimension two bifurcation behaviour, which has been investigated by Tian et al. in ref. [21].

*Corresponding author (email: Q.J.Cao@hit.edu.cn)

The motivation of this paper is to propose a novel oscillator with a pair of irrational nonlinearities, which implies the transition from smooth to discontinuous dynamics. The proposed system can be regarded as a rigid coupling of two separate SD oscillators vibrating horizontally. This simple system has multiple well dynamics [23], high order degenerate singularities [24] and also the transitions between the multiple wells, which imply the multiple stability or from mechanics point of view multiple snap-through bucklings [25,26]. Strong irrational nonlinearities in the presented system may stimulate more research interest in this area, further developments of new methods and also more results in applications in science and engineering. This would enable one to get more insight into the complex dynamics of such nonlinear systems.

2 Mathematical model

In this section, we propose a new nonlinear oscillator which comprises a lumped mass, m, linked by a pair of inclined elastic springs of stiffness k, being capable of resisting both tension and compression and which are pinned to their rigid supports, as shown in Figure 1. Although each of the springs provides linear restoring resistance, the resulting force has a strong irrational nonlinearity due to the geometric configuration. This mechanism is widely found in engineering and physics to model buckled beams [27], folding structures [28] and crystal lattices [9].

The governing equation of this system, which we name as a coupled SD oscillator, can be obtained by employing Lagrange method (see details in Appendix A):

$$mX'' + k(X+a)\left(1 - \frac{1}{\sqrt{(x+a)^2+\beta^2}}\right) + k(X-a)\left(1 - \frac{1}{\sqrt{(x-a)^2+\beta^2}}\right) = 0, \tag{1}$$

where the prime denotes the derivative with respect to time t, m is the lumped mass, X is mass displacement. Each spring is provided with stiffness k and the free length L. a is the half distance between the rigid supports and h is the vertical height.

Eq. (1) can be made dimensionless by letting $\omega_0^2 = 2k/m$, $x = X/L$, $\alpha = a/L$, $\beta = h/L$ and $\tau = \omega_0 t$, written as:

$$\ddot{x} + (x+\alpha)\left(1 - \frac{1}{\sqrt{(x+\alpha)^2+\beta^2}}\right) + (x-\alpha)\left(1 - \frac{1}{\sqrt{(x-\alpha)^2+\beta^2}}\right) = 0, \tag{2}$$

where the dot denotes the derivative with respect to τ. The irrational restoring force

$$F(x,\alpha,\beta) = (x+\alpha)\left(1 - \frac{1}{\sqrt{(x+\alpha)^2+\beta^2}}\right) + (x-\alpha)\left(1 - \frac{1}{\sqrt{(x-\alpha)^2+\beta^2}}\right),$$

models transitions from smooth ($\beta > 0$) to discontinuous ($\beta = 0$) dynamics. It is worth noting that if $\beta = 0$, eq. (2) becomes a discontinuous oscillator:

$$\ddot{x} + 2x - \mathrm{sign}(x+\alpha) - \mathrm{sign}(x-\alpha) = 0. \tag{3}$$

The potential energy of system (2) is written as:

$$V(x) = x^2 - \sqrt{(x+\alpha)^2+\beta^2} - \sqrt{(x-\alpha)^2+\beta^2}$$

and the associated Hamiltonian of system (2) has the following form

$$H(x,y) = \frac{1}{2}y^2 + x^2 - \sqrt{(x+\alpha)^2+\beta^2} - \sqrt{(x-\alpha)^2+\beta^2}.$$

Both smooth and discontinuous resistance forces and their respective potentials are plotted in Figure 2. Figures 2(a) and 2(b) depict the smooth, where Figures 2(c) and 2(d) the discontinuous forces and potentials, respectively. Details regarding the system parameters are given in the corresponding figure caption. It can be seen from Figure 2 that the smooth and discontinuous single, double and triple well potentials can be obtained by varying parameters α and β in system (2).

3 Unperturbed dynamics

In this section, we discuss the complex phase portraits by investigating the equilibrium stability and the bifurcations. System (2) can be rewritten in the following form by letting $\dot{x} = y$,

$$\begin{cases} \dot{x} = y, \\ \dot{y} = -F(x,\alpha,\beta). \end{cases} \tag{4}$$

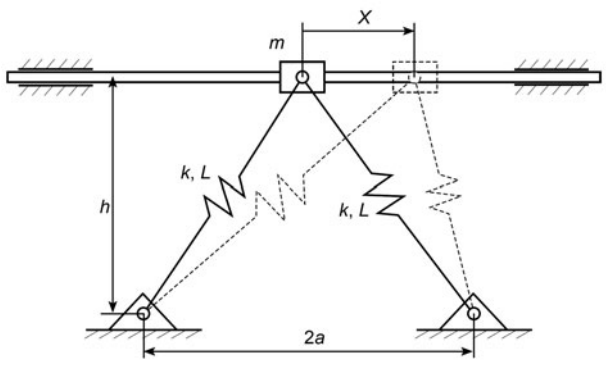

Figure 1 Novel oscillator comprising a lump mass and a pair of linear springs which are obliquely set up.

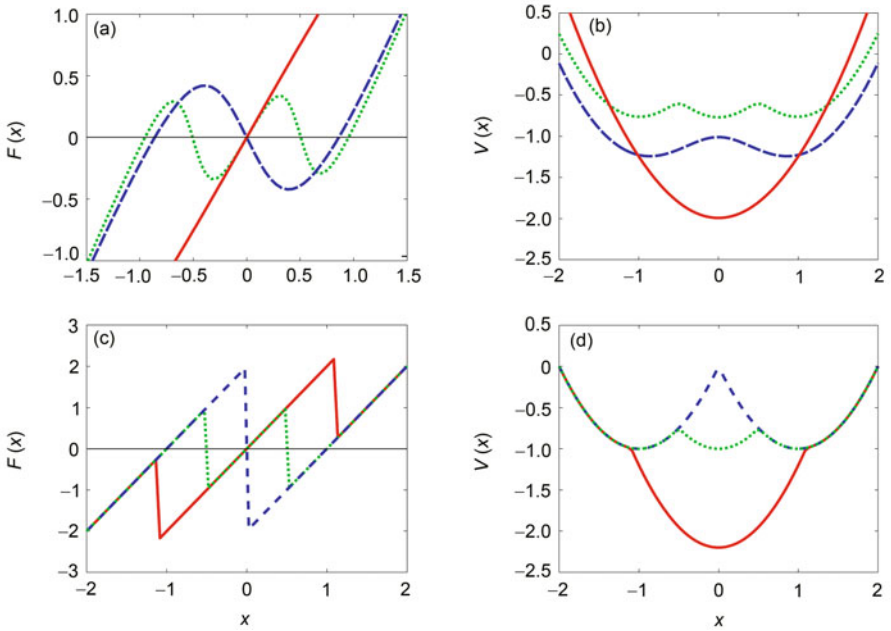

Figure 2 (Color online) Nonlinear restoring forces for the smooth and the discontinuous cases ((a) and (c)), and their corresponding potentials ((b) and (d)). Parameters in (a) and (b) are $\alpha = \beta = 0.25, 0.45, 0.5$ and $\beta = 0, \alpha = 0, 0.25, 0.5$ in (c) and (d). The curves marked with solid red, dashed blue and dotted green represent single, double and triple well dynamics.

3.1 Equilibria bifurcations

It can be seen that the equilibrium set $\{(x,0)|F(x,\alpha,\beta) = 0\}$ of system (4) is a two-dimensional surface in (x,α,β) space, as shown in Figure 3(a). Even if we can not find the analytical form for $x = x(\alpha,\beta)$ explicitly in terms of α and β, we can investigate the structure of the surface by introducing a plane, $\beta = \mu\alpha$, marked in blue, in order to cut the equilibrium surface and intersections are obtained as shown in the following:

$$\begin{aligned}\Sigma_1 &= \{(x,\alpha,\beta)|x \in R, \beta = \mu\alpha, \mu \geqslant 2\},\\ \Sigma_2 &= \{(x,\alpha,\beta)|x \in R, \beta = \mu\alpha, \mu \in (0,2)\},\\ \Sigma_3 &= \{(x,\alpha,\beta)|x \in R, \alpha = 0, \beta > 0\},\end{aligned} \tag{5}$$

which are the subcritical pitchfork and hysteretic bifurcations and the discontinuous bifurcation diagrams, plotted in Figures 3(b)–(d), respectively. The ridge and valley curves of the equilibria surface can be constructed by projecting the surface onto the parametric α-β plane. The transition sets $\Sigma' = C \cup \mathscr{B}_1 \cup \mathscr{B}_2 \cup \mathscr{B}_3$ are obtained and plotted in Figure 4(Σ), where

$$\begin{aligned}\Sigma' &= \{(\alpha,\beta)\,|F = 0, F_x = 0, x \in \mathbf{R}, \alpha, \beta > 0\},\\ \mathscr{B}_1 &= \{(\alpha,\beta)|\ \exists(x,\alpha), \beta > 8\sqrt{5}/25,\ s.t.\ F = F_x = 0\},\\ \mathscr{B}_2 &= \{(\alpha,\beta)|\ \exists(x,\alpha), \beta < 8\sqrt{5}/25,\ s.t.\ F = F_x = 0\},\\ \mathscr{B}_3 &= \{(\alpha,\beta)|\ \exists(x_i,\alpha),\ s.t.\ F = F_x = 0,\ i = 1,2\}.\end{aligned}$$

Here Σ' bifurcates at the catastrophe point $C(\alpha_0,\beta_0) = C\left(4\sqrt{5}/25, 8\sqrt{5}/25\right)$ into three branches of a subcritical pitchfork bifurcation marked as $\mathscr{B}_1$, a supercritical pitchfork bifurcation marked as $\mathscr{B}_2$, and a double saddle-node bifurcation branch denoted by $\mathscr{B}_3$. The transition set Σ', on which the system is structurally unstable, divides the parameters α-β plane into three distinct regions for marked by I, II, and III, as shown in Figure 4(Σ). In each of these regions, the system is structurally stable.

The phase portraits for parameters taken all over the space are plotted in Figure 4 using the Hamiltonian function, H, marked the same as on the corresponding parameter set in the transition sets, Figure 4(Σ). The blue dots are the centres and saddles; the tangent saddle and the centre-saddles connecting the corresponding *homoclinic*, *homo-heteroclinic*, *tangent homoclinic* and *degenerate heteroclinic* orbits are marked with red, as shown in the corresponding plots in Figure 4, where the small circles are the equilibria points of *saddle like* and *centre-saddle like* points connecting the *homoclinic like*, *homo-heteroclinic like* and *heteroclinic like* orbits marked with red.

The bifurcation diagram Figure 4(Σ) shows the transitions from single, double and triple well dynamics, the equilibrium bifurcations of subcritical and supercritical pitchforks and also the transitions of non-buckling to single and double snap-through bucklings. Suppose that a point $M(\alpha,\beta)$ in the parameter plane starting from region I travels anticlockwise along a circumference of a small radius centred at $C(\alpha_0,\beta_0)$ into regions II, II, and finally comes back to I crossing branches $\mathscr{B}_1$, $\mathscr{B}_2$ and $\mathscr{B}_3$ successively. The system behaviour changes dramatically through equilibrium bifurcations, the transitions of multiple well dynamics and singular closed orbits. System (4) bifurcates from a single stable well into a bistable one when $M(\alpha,\beta)$ moves into region II crossing branch $\mathscr{B}_1$ with the subcritical pitchfork, marked with I, $\mathscr{B}_1$ and II, respectively. When $M(\alpha,\beta)$ travels across branch $\mathscr{B}_2$ into region III, system (4) bifurcates into a triple stable well, with the transition from a single into a double snap-

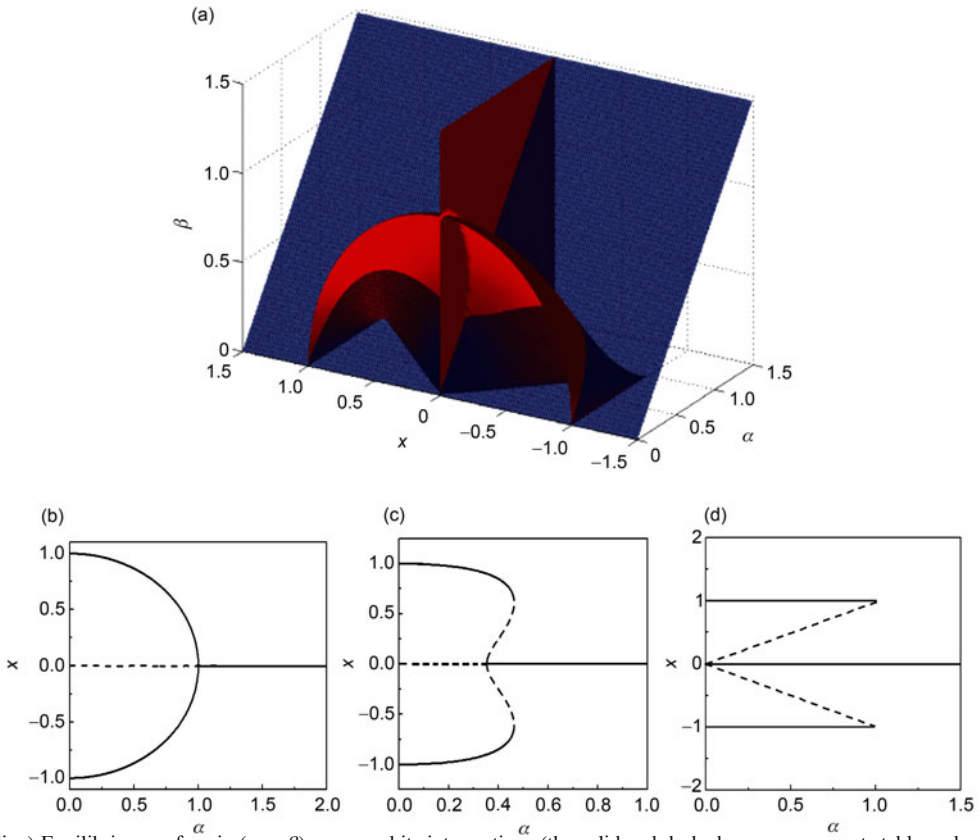

Figure 3 (Color online) Equilibrium surface in (x, α, β) space and its intersections (the solid and dashed curves represent stable and unstable branches). (a) Equilibrium surface, (b) subcritical pitchfork bifurcation, (c) hysteresis bifurcation and (d) the discontinuous bifurcation of 'M' shape.

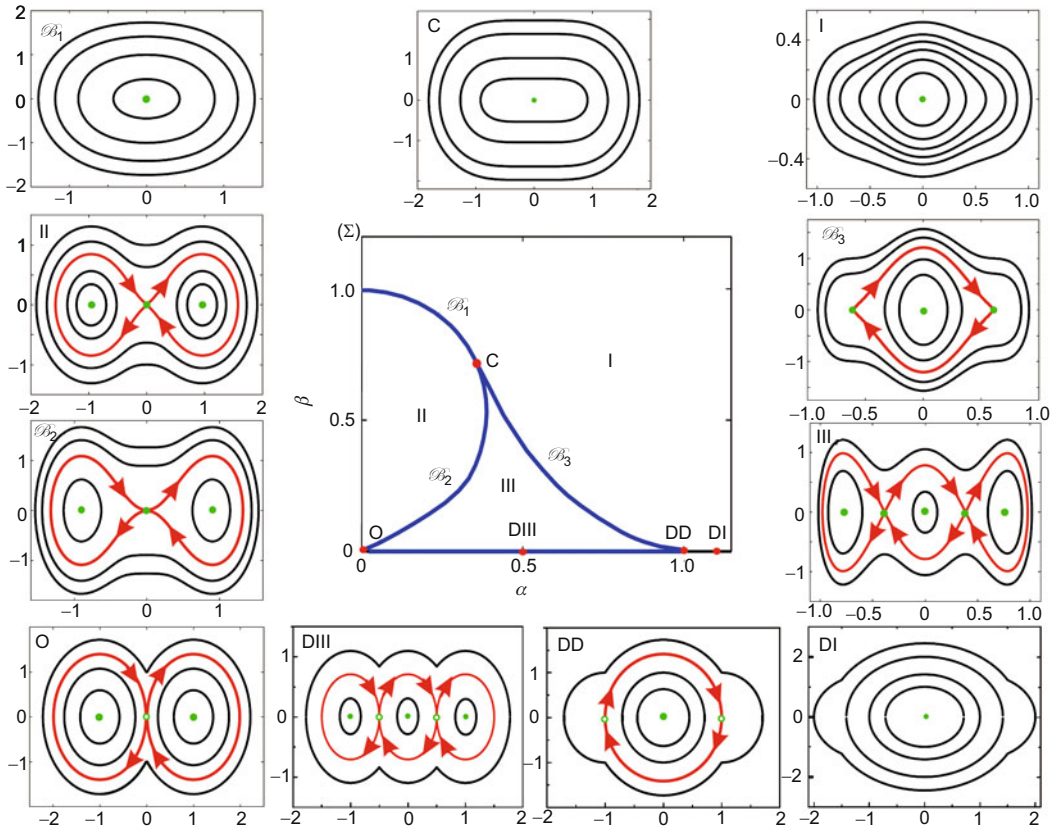

Figure 4 (Color online) Bifurcation diagram and phase portraits. $\sum'$ transition sets divide parameter (α, β) space into three persistent regions, marked I,II and III, for which the corresponding phase portraits I, II, III for persistent, $\mathscr{B}_1, \mathscr{B}_2, \mathscr{B}_3$ for nonpersistent, C for catastrophe point, while O, DI, DD, DIII for discontinuous.

through buckling via a tangent saddle point, which leads to a supercritical pitchfork, as shown in the corresponding pictures, marked with II, $\mathscr{B}_2$ and III respectively. Finally, when $M(\alpha,\beta)$ travels back into region I across $\mathscr{B}_3$, the system becomes again a single stable well via a pair of saddle node bifurcations, as shown in the corresponding pictures, marked with III, $\mathscr{B}_3$ and I, respectively. The phase portrait at the catastrophe point C is also plotted in the top middle panel of Figure 4. Moreover, the discontinuous ($\beta = 0$) phase portraits are presented to show the discontinuous multiple well dynamics, which are marked as O, DIII, DD and DI, respectively.

3.2 Equilibrium stability and singular closed orbits

The main characteristic of the investigated system is strong nonlinearity of irrational type, which possesses both smooth and discontinuous phases depending on the values of the control parameters. There is little possibility to obtain the analytical expressions for both the equilibria and the separatrixes in the smooth regime, as can be seen in ref. [18]. In this subsection, both the equilibrium stability and separatrices are investigated topologically in the smooth regime near the catastrophe point C. A Taylor expansion of the nonlinear resistance force in the neighbourhood of point C is given results in

$$F(x,\alpha,\beta) = 2x - \sum_{n=0}^{\infty}\left[\frac{P_n(\alpha)}{\beta^{n+1}}(x+\alpha)^{n+1} + \frac{P_n(-\alpha)}{\beta^{n+1}}(x-\alpha)^{n+1}\right], \tag{6}$$

where

$$P_n(x) = \frac{1}{2^n n!}\frac{\mathrm{d}^n}{\mathrm{d}x^n}(x^2-1)^n], n = 0,1,2,3,\cdots.$$

Truncating this series to the fifth order (see ref. [35] for details) leads to the topologically equivalent to system (4) near the catastrophe in the smooth regime, which can be written in the following form:

$$\begin{cases}\dot{x} = y\\ \dot{y} = -C_1x - C_3x^3 - C_5x^5,\end{cases} \tag{7}$$

where

$$C_1 = P_1(\alpha) + P_1(-\alpha) = 2 + \frac{2\alpha^2}{(\alpha^2+\beta^2)^{\frac{3}{2}}} - \frac{2}{(\alpha^2+\beta^2)^{\frac{1}{2}}},$$

$$C_3 = P_3(\alpha) + P_3(-\alpha) = \frac{1}{(\alpha^2+\beta^2)^{3/2}} - \frac{6\alpha^2}{(\alpha^2+\beta^2)^{5/2}} + \frac{5\alpha^4}{(\alpha^2+\beta^2)^{7/2}},$$

$$C_5 = P_5(\alpha) + P_5(-\alpha) = -\frac{3}{4}\frac{1}{(\alpha^2+\beta^2)^{5/2}} + \frac{15\alpha^2}{4(\alpha^2+\beta^2)^{7/2}} - \frac{105\alpha^4}{4(\alpha^2+\beta^2)^{9/2}} + \frac{63}{4}\frac{\alpha^6}{(\alpha^2+\beta^2)^{11/2}}.$$

It is not difficult to obtain the transition sets of subcritical $\mathscr{B}_1$, supercritical $\mathscr{B}_2$, and double saddle-node $\mathscr{B}_3$ bifurcations, which model accurately system (4) for the smooth regime. Figure 5(Σ) shows the bifurcation diagram and the corresponding persistent and nonpersistent phase portraits for system (7).

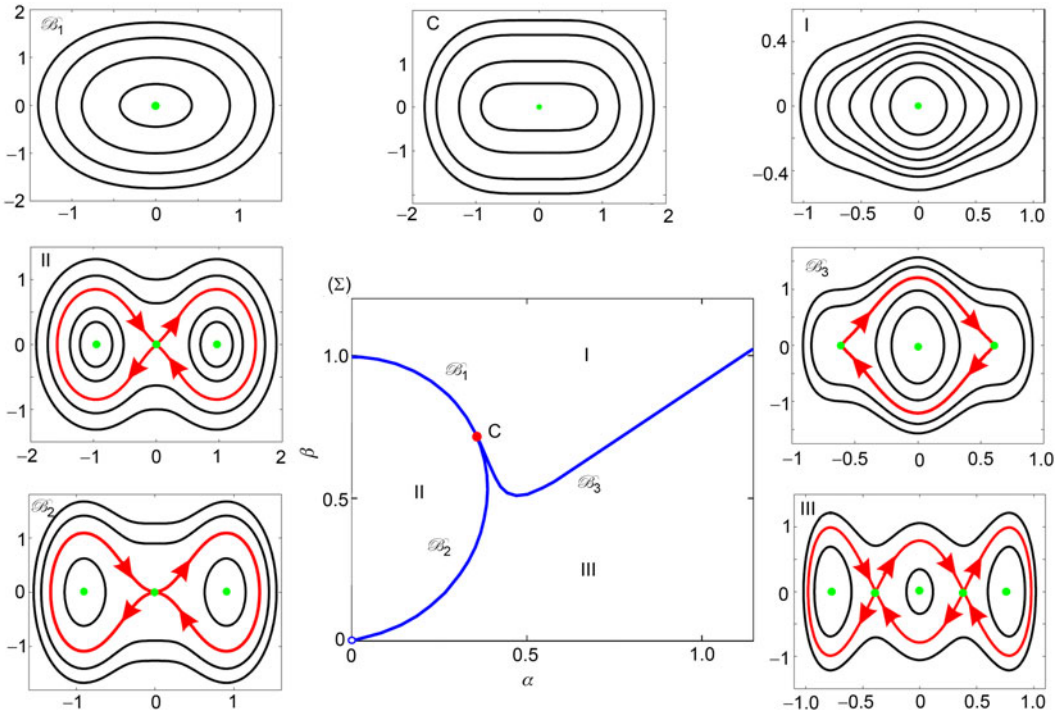

Figure 5 (Color online) Bifurcation diagram and phase portraits of system (7) which is topologically equivalent to system (4) near the catastrophe C. The detailed explanation is the same as in the caption of Figure 4.

The Jacobian of system (7) is obtained and can be written as follows:

$$J_{(x,y)} = \begin{pmatrix} 0 & 1 \\ -C_1 - 3C_3x^2 - 5C_5x^4 & 0 \end{pmatrix},$$

which will be used to investigate the stability in the following discussion. By letting $\dot{x} = 0$, $\dot{y} = 0$, we can obtain five equilibria:

$$P_0 = (0,0), P_1^- = (-x_1, 0), P_1^+ = (x_1, 0),$$
$$P_2^- = (-x_2, 0), P_2^+ = (x_2, 0),$$

where

$$x_1 = \sqrt{(-C_3 - \sqrt{C_3^2 - 4C_1C_5})/2C_5},$$
$$x_2 = \sqrt{(-C_3 + \sqrt{C_3^2 - 4C_1C_5})/2C_5}.$$

The equilibrium stability of system (7) can be obtained by considering the following six cases, which correspond to the respective sets, I, $\mathscr{B}_1$, II $\mathscr{B}_2$, III, and $\mathscr{B}_3$ for different values of parameter α and β.

(1) $C_3 > -2\sqrt{C_1C_5}$ and $C_1, C_5 > 0$

It can be proved that $P_0 = (0,0)$ is the unique equilibrium point of system (7) with the Jacobian

$$J_{(0,0)} = \begin{pmatrix} 0 & 1 \\ -C_1 & 0 \end{pmatrix},$$

whose eigenvalues are $\lambda = \pm i\sqrt{C_1}$, which implies that $(0,0)$ is a centre.

(2) $C_1 = 0, C_3 \geqslant 0$ and $C_5 > 0$

It can be seen that if $(\alpha,\beta) \in \mathscr{B}_1$ for $C_1 = 0, C_3 \geqslant 0$ and $C_5 > 0$, the subcritical pitchfork bifurcation set, and $P_0 = (0,0)$ is also the unique equilibrium with the Jacobian

$$J_{(0,0)} = \begin{pmatrix} 0 & 1 \\ 0 & 0 \end{pmatrix},$$

which implies that $(0,0)$ is a high order degenerated centre (for details see Appendix B). It is worth noting that $C_3 = 0$ implies that at $C\left(4\sqrt{5}/25, 8\sqrt{5}/25\right)$ is a catastrophe.

(3) $C_1 < 0, C_3 \in R$ and $C_5 > 0$

This condition for $(\alpha,\beta) \in$ II, results with three equilibria at

$$P_2^-,\ P_0,\ P_2^+,$$

with the Jacobian at $(0,0)$

$$J_{(0,0)} = \begin{pmatrix} 0 & 1 \\ -C_1 & 0 \end{pmatrix},$$

whose eigenvalues are $\lambda = \pm\sqrt{-C_1}$. This means that $(0,0)$ is a saddle, while P_2^-, P_2^+ are centres. The proof can be found in Appendix B.

It can also be seen that system (7) has a homoclinic orbit which can be expressed as follows:

$$\Gamma_\pm : (x_\pm^{\hom}(t), y_\pm^{\hom}(t)) = (\pm 3x_2^2 e^{-2x_2^2t^2}, \mp 6x_2^4 t e^{-2x_2^2t^2}). \quad (8)$$

(4) $C_1 = 0$, $C_3 < 0$ and $C_5 > 0$

This condition for $(\alpha,\beta) \in \mathscr{B}_2$ gives the supercritical pitchfork bifurcation set, which implies that its equilibria are

$$P_2^-, P_1^- = P_0 = P_1^+, P_2^+,$$

and the Jacobian at $(0,0)$ reads as

$$J_{(0,0)} = \begin{pmatrix} 0 & 1 \\ 0 & 0 \end{pmatrix}.$$

This indicates that (0,0) is a tangent-saddle (see Appendix B for details).

Similarly, the Jacobian of equilibria P_2^- and P_2^+ is obtained and can be written as:

$$J_{P_2^\pm} = \begin{pmatrix} 0 & 1 \\ -2x_2^4 & 0 \end{pmatrix},$$

of which the eigenvalues are $\lambda = \pm i\sqrt{2}x_1^2$, which implies that P_2^- and P_2^+ are centres.

The degenerate homoclinic orbit connecting the tangent saddle can be found, given by

$$\Gamma_\pm : (x_\pm^{\hom}(t), y_\pm^{\hom}(t)) = \left(\pm\frac{\sqrt{6}x_2}{\sqrt{3x_2^4t^2+4}}, \mp\frac{\sqrt{6}x_2^5t}{\sqrt{(3x_2^4t^2+4)^3}}\right). \quad (9)$$

(5) $C_1, C_5 > 0$ and $C_3 < -2\sqrt{C_1C_5}$

In this case for $(\alpha,\beta) \in$ III , system (7) is triple well stable and five distinct equilibria can be found:

$$P_2^-, P_1^-, P_0\ , P_1^+, P_2^+.$$

It is easy to see that P_0 and $P_2^\pm$ are centres and $P_1^\pm$ are saddles, which are connected by a homo-heteroclinc [29,30] orbit, whose branches have the following form:

$$\Gamma_\pm : (x_\pm^{het}(t), y_\pm^{het}(t)) = \left(\pm\frac{\sqrt{2}x_1\sinh(T_1t/2)}{\sqrt{-\xi+\cosh(T_1t)}}, \pm\frac{\sqrt{2}x_1(1-\xi)T_1\cosh(T_1t/2)}{2(-\xi+\cosh(T_1t))^{3/2}}\right),$$
$$\Gamma_\pm : (x_\pm^{\hom}(t), y_\pm^{\hom}(t)) = \left(\pm\frac{\sqrt{2}x_1\cosh(T_1t/2)}{\sqrt{\xi+\cosh(T_1t)}}, \mp\frac{\sqrt{2}x_1(1-\xi)T_1\sinh(T_1t/2)}{2(\xi+\cosh(T_1t))^{3/2}}\right), \quad (10)$$

where $T_1 = x_1^2\sqrt{2C_5(\rho^2-1)}$, $\xi = \frac{5-3\rho^2}{3\rho^2-1}$, $\rho^2 = \frac{-C_3+\sqrt{C_3^2-4C_1C_5}}{-C_3-\sqrt{C_3^2-4C_1C_5}}$.

(6) $C_1, C_5 > 0$ and $C_3 = -2\sqrt{C_1C_5}$

It follows that parameters (α,β) are located in the double saddle-node bifurcation set, $\mathscr{B}_3$, and the equilibria are

$$P_2^- = P_1^-, P_0, P_1^+ = P_2^+,$$

with the Jacobian at $(0,0)$

$$J_{(0,0)} = \begin{pmatrix} 0 & 1 \\ -C_1 & 0 \end{pmatrix},$$

of which the eigenvalues are $\lambda = \pm i\sqrt{C_1}$. This yields $(0,0)$ as a centre.

In the same way, the Jacobian of equilibria $P_2^- = P_1^-, P_1^+ = P_2^+$ can also be obtained and written as:

$$J_{P_{1,2}^{\pm}} = \begin{pmatrix} 0 & 1 \\ 0 & 0 \end{pmatrix},$$

which implies that the pair of equilibria are centre-saddles (see Appendix B), which are connected by a double cuspidal heteroclinic orbit, whose branches are obtained and given by

$$\Gamma_{\pm} : (x_{\pm}^{het}(t), y_{\pm}^{het}(t)) = \left(\pm \frac{x_1^3 t}{\sqrt{x_1^4 t^2 + 3}}, \pm \left(\frac{x_1^3}{\sqrt{x_1^4 t^2 + 3}} - \frac{x_1^7 t^2}{\sqrt{(x_1^4 t^2 + 3)^3}} \right) \right). \quad (11)$$

In summary, the equilibrium stabilities of system (7) are listed in Table 1.

4 Perturbed chaotic thresholds

In this section the chaotic thresholds for system (1) are perturbed by a viscous damping force $\delta X'$, and an external harmonic excitation of amplitude F and frequency Ω are investigated. The perturbed equation is written as follows:

$$mX'' + \delta X' + k(X+a)\left(1 - \frac{L}{\sqrt{(X+a)^2 + h^2}}\right) + k(X-a)\left(1 - \frac{L}{\sqrt{(X-a)^2 + h^2}}\right) = F\cos\Omega t, \quad (12)$$

which can also be made dimensionless by letting $x = y/L, \omega_0^2 = k/m, \alpha = a/L, \beta = h/L, n = \delta/(2m\omega_0)$, $f = F/(kL), \omega = \Omega/\omega_0, \tau = \omega_0 t$, and written as:

$$\ddot{x} + 2n\dot{x} + F(x, \alpha, \beta) = f\cos\omega\tau, \quad (13)$$

where the dot denotes the derivative with respect to τ.

Eq. (13) can be re-written in the following form by letting $\dot{x} = y$,

$$\begin{cases} \dot{x} = y, \\ \dot{y} = -2n\dot{x} - F(x, \alpha, \beta) + f\cos\omega\tau, \end{cases} \quad (14)$$

for which it is impossible to get the analytical thresholds for the perturbed separatrices (see details in ref. [19]).

In the following subsections, we carry out the chaotic analysis for the perturbed system (7) by truncating $F(\alpha, \beta)$ to the fifth order:.

$$\begin{cases} \dot{x} = y, \\ \dot{y} = -2n\dot{x} - C_1 x - C_3 x^3 - C_5 x^5 + f\cos\omega\tau, \end{cases} \quad (15)$$

based upon which Melnikov method can be employed to analyze the chaotic criteria for the singular closed orbits in the following subsections.

4.1 Homoclinic criterion

For a homoclinic orbit of system (7) described in (8) when $C_1 < 0, C_3 \in R$ and $C_5 > 0$, the chaotic threshold of system (15) can be detected by introducing the Melnikov function written as:

$$M_{\pm}^{hom}(\tau) = \int_{-\infty}^{+\infty} -2n(\dot{x}_{\pm}^{hom}(t))^2 \mathrm{d}t + \int_{-\infty}^{+\infty} f\cos\omega(t+\tau)\dot{x}_{\pm}^{hom}(t)\mathrm{d}t. \quad (16)$$

Omitting the tedious calculations leads to

$$M_{\pm}^{hom}(\tau) = \int_{-\infty}^{+\infty} -2n(\dot{x}_{\pm}^{hom}(t))^2 \mathrm{d}t + f\cos\omega\tau \int_{-\infty}^{+\infty} \cos(\omega t)\dot{x}_{\pm}^{hom}(t)\mathrm{d}t - f\sin\omega\tau \int_{-\infty}^{+\infty} \sin(\omega t)\dot{x}_{\pm}^{hom}(t)\mathrm{d}t.$$

Let us define

$$R^0(\omega) = \frac{\int_{-\infty}^{+\infty} (\dot{x}_{\pm}^{hom}(t))^2 \mathrm{d}t}{\int_{-\infty}^{+\infty} \cos\omega(t+\tau)\dot{x}_{\pm}^{hom}(t)\mathrm{d}t}, \quad (17)$$

which provides a way to detect chaotic motion for a homoclinic orbit which is similar to the standard Duffing homoclinic orbit by using the condition: $f/2n > R^0(\omega)$ (see [30] for details). This implies that the roots of $M_{\pm}^{hom}(\tau)$ are simple, which enables transverse intersections between stable and unstable manifolds of a tangent saddle to possibly occur and system (15) can be chaotic. The detected chaotic threshold is presented in Figure 6(a).

In order to verify the criterion obtained in this subsection, a numerical simulation was carried out by fixing parameter

Table 1 Stability analysis for equilibria of system (7)

α, β	C_1, C_2, C_3	Equilibrium	Singularity
I	$C_1, C_5 > 0$ and $C_3 < -2\sqrt{C_1 C_5}$	P_0	P_0 centre
$\mathscr{B}_1$	$C_1 = 0, C_3 \geqslant 0$ and $C_5 > 0$	P_0	P_0 centre
II	$C_1 < 0, C_3 \in R$ and $C_5 > 0$	P_2^-, P_0, P_2^+	P_0 saddle, $P_2^{\pm}$ centre
$\mathscr{B}_2$	$C_1 = 0, C_3 < 0$ and $C_5 > 0$	$P_2^-, P_1^- = P_0 = P_1^+, P_2^+$	P_1^-, P_0, P_1^+ saddle, $P_2^{\pm}$ centre
III	$C_1, C_5 > 0$ and $C_3 < -2\sqrt{C_1 C_5}$	$P_2^-, P_1^-, P_0, P_1^+, P_2^+$	P_0, $P_2^{\pm}$centre,$P_1^{\pm}$ saddle
$\mathscr{B}_3$	$C_1, C_5 > 0$ and $C_3 = -2\sqrt{C_1 C_5}$	$P_2^- = P_1^-, P_0, P_1^+ = P_2^+$	P_0 centre, $P_1^{\pm}$=$P_2^{\pm}$ centre-saddle

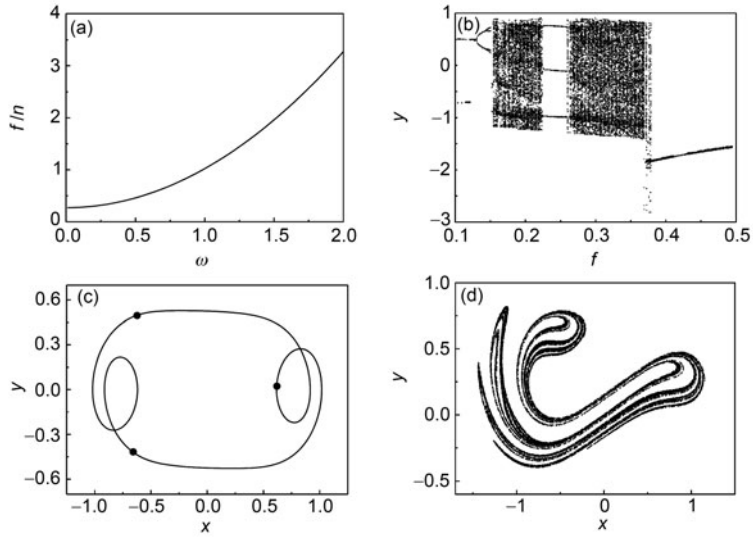

Figure 6 (a) Homoclinic orbits chaotic boundary for system (15) in the $(\omega, f/n)$ plane, (b) bifurcation diagram of f versus y, (c) period three motion for f=0.23 and (d) chaotic attractor for f=0.3.

$\alpha = 0.3, \beta = 0.6, n = 0.05, \omega = 1.0$. A bifurcation diagram, y versus f, is given in Figure 6(b), from which periodic windows and chaotic regions can be clearly seen as parameter f changes. Figures 6(c) and 6(d) plot the phase portrait of a period three solution for $f = 0.23$ and a chaotic attractor for f= 0.3, respectively.

4.2 Tangent homoclinic criterion

The chaotic threshold of system (15) of the tangent homoclinic orbit described by (9) of system (7) when $C_1 = 0$ $C_3 < 0$ and $C_5 > 0$ can be detected by introducing the following Melnikov function (the Melnikovian)

$$M_{\pm}^{hom}(\tau) = \int_{-\infty}^{+\infty} -2n(\dot{x}_{\pm}^{hom}(t))^2 \mathrm{d}t + \int_{-\infty}^{+\infty} f\cos\omega(t+\tau)\dot{x}_{\pm}^{hom}(t)\mathrm{d}t,$$

and then

$$M_{\pm}^{hom}(\tau) = \int_{-\infty}^{+\infty} -2n(\dot{x}_{\pm}^{hom}(t))^2 \mathrm{d}t + f\cos\omega\tau\int_{-\infty}^{+\infty}\cos(\omega t)\dot{x}_{\pm}^{hom}(t)\mathrm{d}t - f\sin\omega\tau\int_{-\infty}^{+\infty}\sin(\omega t)\dot{x}_{\pm}^{hom}(t)\mathrm{d}t.$$

As in subsect. (4.1), we define

$$R^0(\omega) = \frac{\int_{-\infty}^{+\infty}(\dot{x}_{\pm}^{hom}(t))^2\mathrm{d}t}{\int_{-\infty}^{+\infty}\cos\omega(t+\tau)\dot{x}_{\pm}^{hom}(t)\mathrm{d}t}, \tag{18}$$

which allows us to detect chaos for the pertgurbed homoclinic orbit with a tangent saddle by using the condition $f/2n > R^0(\omega)$. The Melnikovian detecting chaotic boundary is shown in Figure 7(a).

Again numerical simulation was carried out to verify the efficiency of the criterion, for parameters $\alpha = \beta = 0.3559, n = 0.005$ and $\omega = 0.5$ being fixed. A bifurcation diagram y versus f is given in Figure 7(b), where chaotic behaviour and periodic windows are clearly seen. Figures 7(c) and 7(d) dipict the chaotic attractor and period three motion.

4.3 Homo-heteroclinic criteria

Similarly as for the homo-heteroclinic orbit of system (7) described by eq. (10) when $C_1, C_5 > 0$ and $C_3 < -2\sqrt{C_1C_5}$, the chaotic threshold of system (15) can be detected by introducing the Melnikov function

$$M_{\pm}^{het}(\tau; f, \omega, n) = \int_{-\infty}^{+\infty} -2n(\dot{x}_{\pm}^{het}(t))^2\mathrm{d}t + \int_{-\infty}^{+\infty} f\cos\omega(t+\tau)\dot{x}_{\pm}^{het}(t)\mathrm{d}t,$$

which yields

$$M_{\pm}^{het}(\tau; f, \omega, n) = \int_{-\infty}^{+\infty} -2n(\dot{x}_{\pm}^{het}(t))^2\mathrm{d}t - f\sin\omega\tau\int_{-\infty}^{+\infty}\sin(\omega t)\dot{x}_{\pm}^{het}(t)\mathrm{d}t + f\cos\omega\tau\int_{-\infty}^{+\infty}\cos(\omega t)\dot{x}_{\pm}^{het}(t)\mathrm{d}t.$$

The evaluation of this integral leads to the following Melnikov function as in ref. [26]. We define

$$R_{het}^0(\omega) = \frac{\int_{-\infty}^{+\infty} -2n(\dot{x}_{\pm}^{het}(t))^2\mathrm{d}t}{\int_{-\infty}^{+\infty} f\cos\omega(t+\tau)\dot{x}_{\pm}^{het}(t)\mathrm{d}t} = \frac{T_1^2}{8\omega\pi(\xi+1)}\left[\frac{(2\xi)}{(1-\xi^2)^{1/2}}\left(\arcsin\xi+\frac{\pi}{2}\right) + 2 + \xi\right]\sinh\left(\frac{2\omega}{T_1}\right),$$

which determines a possible chaos if $f/2n > R_{het}^0(\omega)$, which is shown in Figure 8(a) by the dashed curve.

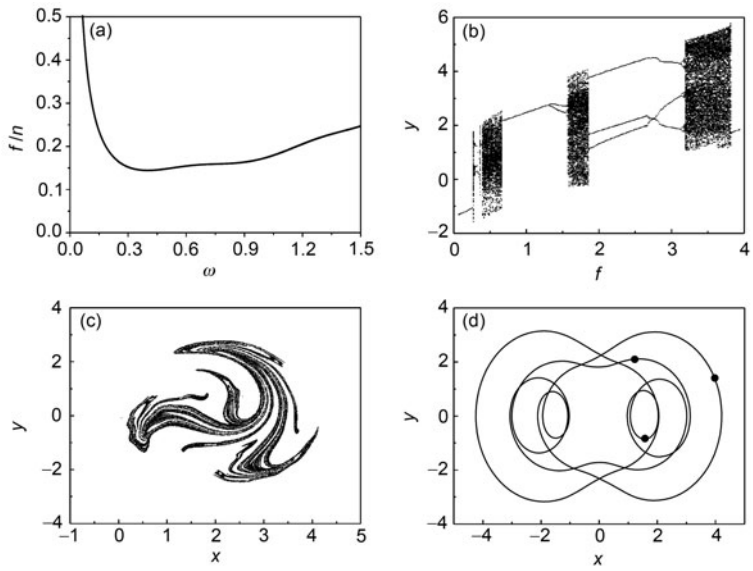

Figure 7 (a) Melnikovian chaotic boundary for the degenerate homoclinic orbits with a tangent saddle for system (15) in the $(\omega, f/n)$ plane, (b) bifurcation diagram of y versus f, (c) a chaotic attractor for f=1.8 and (d) a period three for $f = 2.2$.

Next we focus our attention on the homoclinic branches, and the corresponding Melnikov integral has the following form

$$M_{\pm}^{hom}(\tau) = \int_{-\infty}^{+\infty} -2n(\dot{x}_{\pm}^{hom}(t))^2 \mathrm{d}t + f\cos\omega\tau \int_{-\infty}^{+\infty} \cos(\omega t)\dot{x}_{\pm}^{hom}(t)\mathrm{d}t - f\sin\omega\tau \int_{-\infty}^{+\infty} \sin(\omega t)\dot{x}_{\pm}^{hom}(t)\mathrm{d}t.$$

The calculation of the above integral leads to the Melnikov function described in[27], where we define

$$R_{hom}^{0}(\omega) = \frac{\int_{-\infty}^{+\infty} -2n(\dot{x}_{\pm}^{hom}(t))^2\mathrm{d}t}{\int_{-\infty}^{+\infty} f\cos\omega(t+\tau)\dot{x}_{\pm}^{hom}(t)\mathrm{d}t} = \frac{T_1^2}{32\omega\pi(\xi+1)}\left[\frac{(2\xi)}{(1-\xi^2)^{1/2}}\left(\arcsin\xi - \frac{\pi}{2}\right) + 2 + \xi\right]\cosh\left(\frac{2\omega}{T_1}\right),$$

which allows to calculate the analytical chaotic threshold of system (15) for $f/2n > R_{hom}^{0}(\omega)$ plotted in Figure 8(a) with a solid curve.

The parameters $\alpha = \beta = 0.4348, n = 0.01$ and $\omega = 0.4$ are kept fixed in this numerical analysis. The bifurcation diagram of system (13), x versus f, is shown in Figure 8(b). Examples of a period two and a chaotic attractor are plotted in Figure 8(c) and Figure 8(d), respectively.

4.4 Cuspidal heteroclinic criterion

In the same way, the chaotic criterion for system (15) to determine the cuspidal heteroclinic orbit of system (7) described by (11) for $C_1, C_5 > 0$ and $C_3 = -2\sqrt{C_1C_5}$ can be obtained by employing the Melnikov function as in the following.

$$M_{\pm}^{het}(\tau, f, \omega, n) = \int_{-\infty}^{+\infty} -2n(\dot{x}_{\pm}^{het}(t))^2\mathrm{d}t + \int_{-\infty}^{+\infty} f\cos\omega(t+\tau)\dot{x}_{\pm}^{het}(t)\mathrm{d}t,$$

which can be integrated for both orbits, the upper one and the lower to obtain the chaotic thresholds. Without loss of generality, we only present the Melnikov function for the upper heteroclinic orbit, which is time-independent and depends only on two parameters, f and n, respectively.

$$M_{\pm}^{het}(\tau, f, \omega, n) = \int_{-\infty}^{+\infty} -2n(\dot{x}_{\pm}^{het}(t))^2\mathrm{d}t + f\cos\omega\tau \int_{-\infty}^{+\infty} \cos(\omega t)\dot{x}_{\pm}^{het}(t)\mathrm{d}t - f\sin\omega\tau \int_{-\infty}^{+\infty} \sin(\omega t)\dot{x}_{\pm}^{het}(t)\mathrm{d}t.$$

Let us define

$$R^{0}(\omega) = \frac{\int_{-\infty}^{+\infty} (\dot{x}_{\pm}^{het}(t))^2\mathrm{d}t}{\int_{-\infty}^{+\infty} \cos\omega(t+\tau)\dot{x}_{\pm}^{het}(t)\mathrm{d}t}, \tag{19}$$

which follows the analytical chaos criterion for the degenerate orbit for $f/2n > R^{0}(\omega)$.

Numerical simulation was carried out to verify the efficiency of the criteria for the parameters $\alpha = 0.4654$, $\beta = 0.4654$, $n = 0.005$ and $\omega = 0.33$ kept fixed. The bifurcation diagram of system (13), x versus f, is plotted in Figure 9(b). When f increases beyond above the threshold value and reaches $f = 0.15$, system (13) jumps to the area of chaotic motion. As f increases, a period-doubling bifurcation starts from $f = 0.19$ and other chaotic area starts from $f = 0.22$, as be observed in Figure 9(b). It can also be seen from this bifurcation diagram, that a period-five window occurs when f takes values between 0.26 and 0.28. Figures 9(c) and 9(d) plot a chaotic attractor for $f = 0.252$ and a phase portrait for a period-five motion for $f = 0.275$, respectively.

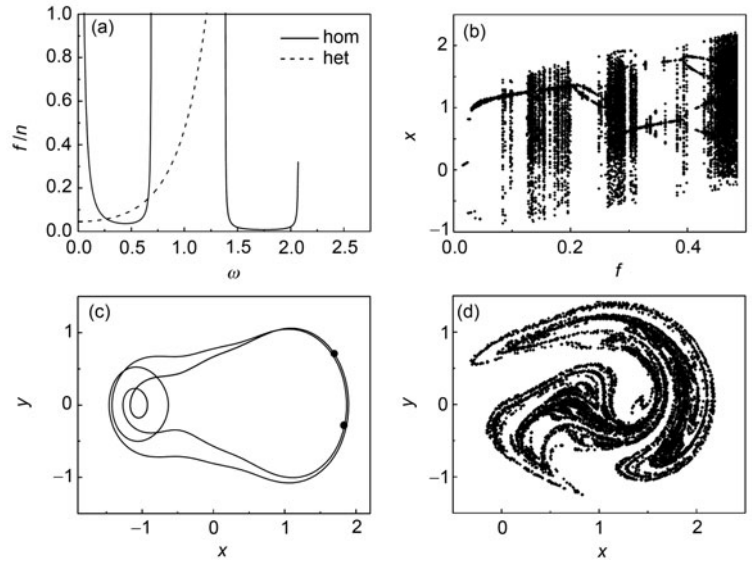

Figure 8 (a) Chaotic thresholds for the homo-heteroclinic orbits: the bold curves stand for the homoclinic branches and the dashed for the heteroclinic branches of system (15) in the $(\omega, f/n)$ plane. The bold curves indicate the homoclinic and the dotted marks the heteroclinic Melnikov boundaries. (b) Bifurcation diagram for f versus x, (c) period-2 solution for $f = 0.42$ and (d) chaotic attractor for f =0.47.

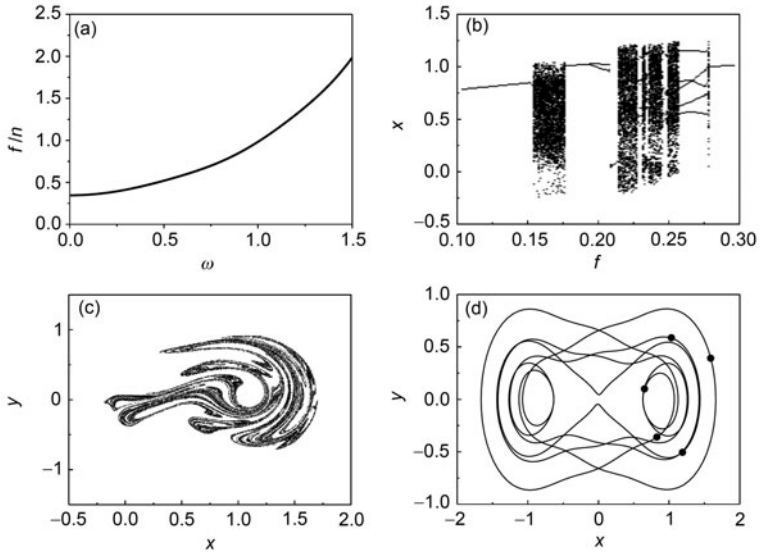

Figure 9 (a) Melnikov chaotic boundary for the double cuspidal heteroclinic orbits, $\omega - f/n$ curve for system (15), (b) bifurcation diagram, x versus f, (c) chaotic attractor calculated for $f = 0.252$ and (d) period five motion calculated for $f = 0.275$.

5 Conclusions

In this paper, we have proposed a novel nonlinear oscillator with strong irrational nonlinearities, which demonstrates s both standard ($\beta > 0$) and non-standard ($\beta = 0$) responses of single, double and triple well dynamics. The equilibrium stability and the bifurcation structure have been investigated showing the subcritical, supercritical pitchforks and saddle-node bifurcations. Phase portraits have also been plotted to demonstrate the complex transitions from the multiple well dynamics, singular closed orbits and the associated snap-through bucklings as well for the unperturbed system. The Melnikov method has been successfully employed to derive the analytical chaotic criteria for the existing singular closed orbits when the system is perturbed by viscous damping force and external harmonic excitation.

The nonlinear oscillator proposed herein in this paper is being actively studied in two main directions. First, the unknown properties at the limit of $\beta = 0$ are analyzed to better understand the bifurcation structure being perturbed by damping and external forcing. The second direction is the Hopf bifurcations and higher codimension [31,32] analysis near the catastrophe point C.

Appendix A

Consider an oscillator which is composed of a lump mass of m and a pair of linear springs of stiffness k, as illustrated in Figure 1. The kinetic energy and the potential energy of the system can be written as:

$$T = mX'^2/2,$$

and

$$V = k(\sqrt{(X+a)^2+h^2} - L)^2/2 + k(\sqrt{(X-a)^2+h^2} - L)^2/2,$$

which follows the Lagrangian formulation,

$$\frac{\mathrm{d}L}{\mathrm{d}t}\left(\frac{\partial L}{\partial X'}\right) - \frac{\partial L}{\partial X} = 0,$$

where $L = T - V$, and

$$\frac{\partial L}{\partial X'} = mX'$$

$$\frac{\partial L}{\partial X} = -k(X+a)\left(1 - \frac{L}{\sqrt{(X+a)^2+h^2}}\right) - k(X-a)\left(1 - \frac{L}{\sqrt{(X-a)^2+h^2}}\right).$$

The equation of motion for the system can be obtained and written as follows:

$$mX'' + k(X+a)\left(1 - \frac{L}{\sqrt{(X+a)^2+h^2}}\right) + k(X-a)\left(1 - \frac{L}{\sqrt{(X-a)^2+h^2}}\right) = 0.$$

Appendix B

Consider the differential equation:

$$\ddot{x} + f(x) = 0, \tag{a1}$$

or the first order equivalent system

$$\begin{cases} \dot{x} = y, \\ \dot{y} = -f(x). \end{cases} \tag{a2}$$

Here $f(x)$ can be expanded into a Taylor series in the neighborhood of $x = 0$,

$$f(x) = f(0) + f'(0) + \frac{f''(0)}{2!} + \frac{f'''(0)}{3!} + \cdots + \frac{f^{(n)}(0)}{n!} + o(x^n). \tag{a3}$$

Substituting (a3) into system (a2) yields

$$\begin{cases} \dot{x} = y, \\ \dot{y} = l_0 + l_1 x + l_2 x^2 + l_3 x^3 + \cdots + l_n x^n + o(x^n). \end{cases} \tag{a4}$$

where $l_n = -\frac{f^{(n)}(0)}{n!}$ is called the Lyapunov measure [33].

The degenerate equilibria ($n > 1$) of system (a2) can be classified as follows:

(1) The equilibrium is a center-saddle if the first indicator of non-zero Lyapunov measure ($l_{2p} \neq 0, p = 0, 1, \cdots$) is even, as shown in Figures A1(a) and (b); (2) The equilibrium is a saddle or a tangent-saddle if the first non zero Lyapunov measure is positive and the indicator is odd ($l_{2p+1} > 0, p = 0, 1, \cdots$), See Figure 10(c); (3) The equilibrium is a high order degenerate centre if the first non zero Lyapunov measure is negative and the indicator is odd ($l_{2p+1} < 0, p = 0, 1, \cdots$), See Figure 10(d).

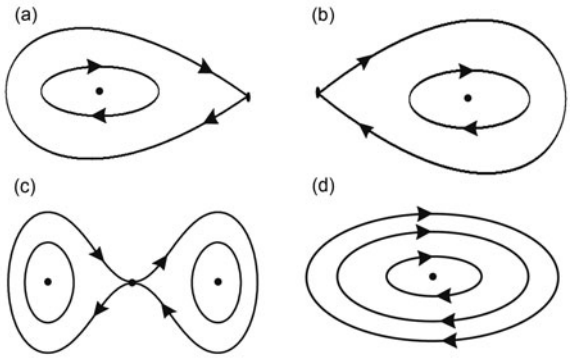

Figure A1 Phase portraits for different Lyapunov measures: (a) and (b) centre-saddle for $l_{2p} \neq 0$; (c) degenerate or tangent saddle for $l_{2p+1} > 0$, and (d) $l_{2p+1} < 0$.

This work was supported by the National Natural Science Foundation of China (Grant No. 10872136, 11072065 and 10932006).

1 Field S, Kaus M, Moore M G. Chaotic system of falling disc. Nature, 1997, 388: 252–254
2 Lenci S, Rega G. Regular nonlinear dynamics and bifurcations of an impacting system under general periodic excitation. Nonlin Dyn, 2003, 34: 249–268
3 Perter L V, Gabor D. Symmetry, optima and bifurcation is structure design. Nonlin Dyn, 2006, 43: 47–58
4 Padthe A K. Feedback stabilization of snap-through buckling in a preloaded two-bar linkage with hysteresis. Int J Nonlin Mech, 2008, 43: 277–291
5 Avramov K V, Mikhlin Y V. Snap-through truss a vibration absorber. J Vib Control, 2004, 10: 291–308
6 Brenna M J, Elliott S J, Bonello P, et al. The "click" mechanism in dipteran flight: if it exists, then what effect does it have. J Theor Biol, 2003, 22: 205–213
7 Matin L, Daniel J G C, Jean F J, et al. Membrane buckling induced by curved filaments. Phys Rev Lett, 2009, 103: 38101–38104
8 Xie Y D. Elliptic function waves of spinor Bose-Einstein condensates in an optical lattice. Commun Theor Phys, 2009, 51: 445–449
9 Toda M. Theory of Nonlinear Lattices. New York: Springer-Verlag, 1978
10 Stewart I. Quantizing the classical cat. Nature, 2004, 430: 731–732
11 Doupac M, Beale D G, Overfelt R A. Three-dimensional lumped mass/lumped spring modeling and nonlinear behaviour of a levitated droplet. Nonlin Dyn, 2005, 42: 25–42
12 Kaper H G. The behaviour of a mass-spring system provided with a discontinuous dynamic vibration absorber. Appl Sci Res A, 1961, 10: 369–383
13 Boubaker B B, Haussy B. Mesoscopic fabric models using a discrete mass-spring approach: Yarn-yarn interactions analysis. J Mater Sci, 2005, 40: 5925–5932
14 Terumichi Y, Ohtsuka M, Yoshizava M, et al. Nonstationary vibrations of a string with time-varying length and a mass-spring system attached at the lower end. Nonlin Dyn, 1997, 12: 39–55
15 Cao Q J, Wiercigroch M, Pavlovskaia E E, et al. Archetypal oscillator for smooth and discontinuous dynamics. Phys Rev E, 2006, 74: 046218

16 Cao Q J, Wiercigroch M, Pavlovskaia E E, et al. Piecewise linear approach to an archetypal oscillator for smooth and discontinuous dynamics. Phil Trans R Soc A, 2008, 366: 635–652
17 Cao Q J, Wiercigroch M, Pavlovskaia E E, et al. The limit case response of the archetypal oscillator for smooth and discontinuous dynamics. Int J Nonlin Mech, 2008, 43: 462–473
18 Cao Q J, Han N. A rotating pendulum linked by an oblique spring. Chin Phys Lett, 2011, 28: 060502
19 Cao Q J, Xiong Y P, Wiercigroch M. Resonances behavior of SD oscillator at the discontinuous phases. J Appl Anal Comput, 2011, 1: 183–191
20 Tian R L, Cao Q J, Li Z X. Hopf bifurcations for the recently proposed smooth-and-discontinuous oscillator. Chin Phys Lett, 2010, 27: 074701
21 Tian R L, Cao Q J, Yang S P. The codimension-two bifurcation for the recent proposed SD oscillator. Nonlin Dyn, 2010, 59: 19–27
22 Lai S K, Xiang Y. Application of a generalized Senator-Bapat perturbation technique to nonlinear dynamical systems with an irrational restoring force. Comput math Appl, 2010, 60: 2078–2086
23 Zheng W M, Halsall M P , Harrison P, et al. Far-infrared absorption studies of Be acceptors in δ-doped GaAs/AlAs multiple quantum wells. Sci China Ser G, 2006, 49: 702–708
24 Gini J, Llibre J. Integrability, degenerate centers, and limit cycles for a class of polynomial differential systems. Comput Math Appl, 2006, 51: 1453–1462
25 Feodosev V I. Selected problems in Engineering Mechanics. Moscow: Nauka, 1980
26 Gulyev V I, Bazhenov V A, Popov S L. Applied Problems in Theory of Nonlinear Oscillations of Mechanical system. Moscow: Vysshaya Shkola, 1989
27 Sorokin S V, Terentiev A V. On modal interaction, stability and nonlinear dynamics of a modal two D. O. F. mechanical system performing snap-through motion. Nonlin Dyn, 1998, 16: 239–257
28 Ario I, Watson A. Structural stability of multi-folding structures with contact problem. J Sound Vib, 2009, 324: 263–282
29 Han M A, Zhang H, Yang J M. Limit cycle bifurcations by perturbing a cuspidal loop in a Hamilton system. J Diff Equ, 2009, 246: 129–163
30 Moon F C, Holmes P J. A magneto elastic strange attractor. J Sound Vib, 1979, 65: 275–296
31 Golubitsky M, Schaeffer D G, Stewart I. Singularities and Groups in Bifurcations Theory, I. New York: Springer-Verlag, 1985
32 Chen Y S, Xu J, Universal classifications of the prime prametric resonance of van de Pol Duffing-Mathieu type. Sci China Ser A-Math Phys Astron, 1995, 38: 1287–1297
33 Shilnikov L P, Shilnikov A L, et al. Methods of Qualitative Theory in Nonlinear Dynamics, part II. Singapore: World Scientific, 2001